

# Photonic Generation of Chirped Millimeter-Wave Pulses Based on Nonlinear Frequency-to-Time Mapping in a Nonlinearly Chirped Fiber Bragg Grating

Chao Wang and Jianping Yao, *Senior Member, IEEE*

**Abstract**—A novel approach to optically generating chirped millimeter-wave pulses with tunable chirp rate based on spectral shaping and nonlinear frequency-to-time mapping is proposed and experimentally demonstrated. In the proposed approach, the optical power spectrum of an ultrashort pulse from a femtosecond pulsed laser is shaped by a two-tap Sagnac loop filter that has a sinusoidal frequency response. The spectrum-shaped optical pulse is then sent to a nonlinearly chirped fiber Bragg grating (NL-CFBG) with a tunable nonlinear group delay to serve as a high-order dispersive device to perform the nonlinear frequency-to-time mapping. A chirped electrical pulse with a high central frequency and large chirp rate is then generated at the output of a high-speed photodetector. The NL-CFBG used in the proposed system is produced from a regular linearly chirped fiber Bragg grating based on strain-gradient beam tuning. A detailed theoretical analysis on the chirped pulse generation is developed, which is verified by numerical simulations and experiments. Millimeter-wave pulses with a central frequency of around 35 GHz and instantaneous frequency chirp rates of 0.053 and 0.074 GHz/ps are experimentally generated.

**Index Terms**—Chirped pulse generation, chromatic dispersion, frequency-to-time mapping, microwave photonics, nonlinearly chirped fiber Bragg grating (NL-CFBG), pulse compression, radar.

## I. INTRODUCTION

**I**N MODERN radar systems, pulse compression techniques using frequency-chirped or phase-encoded pulses have been widely used to improve the radar range resolution [1], where the pulsewidth is significantly compressed at the receiver end by matched filtering. Chirped electrical pulses have also found their applications in spread-spectrum communications and in chirp pulse microwave computed tomography [2]. Conventionally, a chirped electrical pulse is generated in the electrical domain using electronic circuitry [3], [4]. However, the major limitation associated with the electrical technique is the low central frequency. At the current stage of development of radar and communications systems, a central frequency up to the tens or even hundreds of gigahertz is often required [1].

Manuscript received August 18, 2007; revised October 29, 2007. This work was supported by the Natural Sciences and Engineering Research Council of Canada (NSERC).

The authors are with the Microwave Photonics Research Laboratory, School of Information Technology and Engineering, University of Ottawa, Ottawa, ON, Canada K1N 6N5 (e-mail: jpyao@site.uOttawa.ca).

Color versions of one or more of the figures in this paper are available online at <http://ieeexplore.ieee.org>.

Digital Object Identifier 10.1109/TMTT.2007.914639

An efficient solution to generate electrical pulses with a high frequency is to use optical techniques [5]–[7]. Optical spectral shaping of a broadband ultrashort pulse followed by frequency-to-time mapping in a dispersive element has been demonstrated to be a viable technique to generate high-frequency electrical pulses with arbitrary waveform. In an optical spectral shaping system, a spatial light modulator [5] or a fiber-optic spectral filter [6], [7] is usually used to shape the optical spectrum of an ultra-narrow pulse. By properly designing the frequency response of the optical spectral filter, an electrical pulse with the shape identical to the shaped spectrum is obtained after the frequency-to-time mapping. A key feature of this technique is that the temporal pulse shaping is done in the frequency domain, which is easy to implement using a spectral filter. In addition, if the spectral response of the filter is changed, the shape of the generated electrical pulse is also changed, and the system is reconfigurable. The frequency- to time-domain mapping relationship is only determined by the system dispersion [8]. Recently, an all-optical method to generate linearly chirped microwave pulses was demonstrated, which was based on the interference of two optical pulses that were generated based on spectrum filtering and frequency-to-time mapping using two linearly chirped fiber Bragg gratings with different chirp rates [9]. Due to the constant first-order dispersion provided by the two chirped gratings, chirped pulses with only a fixed chirp rate were generated. In addition, since the system was based on optical interference in a Mach–Zehnder interferometer (MZI), it is sensitive to environmental perturbations.

In most of the previous studies, the dispersive device used to perform the frequency-to-time mapping was a length of single-mode fiber [7] or a linearly chirped fiber Bragg grating [8]. Since the high-order dispersion of the dispersive device is negligible within the pulse spectral bandwidth, only linear frequency-to-time mapping could be realized. In other words, only chirp-free electrical pulses can be generated using a dispersive device with only the first-order dispersion if the optical spectral filter has a uniform sinusoidal spectral response [6]. Therefore, to generate chirped electrical pulses, one may use either a uniform sinusoidal spectral filter with a dispersive device having both the first- and second-order dispersion, or an optical spectral filter with chirped spectral response with a dispersive device having only the first-order dispersion. In this paper, we assume that the optical filter has a uniform sinusoidal response, which is much easier to implement than the optical filter with a chirped spectral response. Therefore, our efforts will be directed to in-

investigate the use of a nonlinearly chirped fiber Bragg grating (NL-CFBG) with a tunable high-order dispersion for the generation of chirped millimeter-wave pulses. Although second-order dispersion-induced pulse chirping was observed with a very long single-mode fiber [10], the system has an obvious limitation: the second-order dispersion of a single mode fiber is very small; to obtain a large second-order dispersion, a very long fiber is required, which makes the system bulky. In addition, in a long fiber, the effect of polarization mode dispersion cannot be ignored, which would affect the performance of the generation system. Compared with the system in [10], the use of an NL-CFBG instead of a long single-mode fiber makes the system more compact, and more importantly, enables a flexible dispersion management. The NL-CFBG used in the proposed system is produced from a regular linearly chirped fiber Bragg grating using a simple and low-cost technique based on strain-gradient beam tuning. Although the technique has been used to convert a uniform fiber Bragg grating to a linearly chirped fiber Bragg grating [11], to the best of our knowledge, it is the first time that the technique is used to convert a linearly chirped fiber Bragg grating to an NL-CFBG.

Some preliminary research has been recently reported by us [12], [13] with the results obtained mainly based on very preliminary experimental observations, where a chirped electrical pulse with only a fixed chirp rate was generated. In addition, a theoretical investigation on the chirped microwave pulse generation using an NL-CFBG with an emphasis on the understanding of the influence of the group delay ripples in an NL-CFBG on the pulse generation performance was recently implemented in [14]. To have a better understanding of the chirped electrical pulse generation technique and to study the feasibility of the technique for practical implementation, we believe that an in-depth theoretical analysis with experimental verifications is necessary.

In our proposed system, an optical sinusoidal spectrum is obtained by spectrally filtering a broadband transform-limited ultrashort optical pulse using a two-tap Sagnac loop filter. The generation of a chirped millimeter-wave pulse is then realized by nonlinear frequency-to-time mapping in an NL-CFBG. The central frequency of the generated chirped pulse is dependent upon the first-order dispersion of the NL-CFBG for an Sagnac loop filter with a given free spectral range (FSR), whereas the chirp rate of the generated pulse is determined by both the first- and high-order dispersion. Since the dispersion of the NL-CFBG can be easily controlled, our approach provides the flexibility to tailor the frequency profile of the generated chirped millimeter-wave pulses, such as the central frequency and chirp rate. In addition, since no MZI-based optical interference is involved in the approach, the system is more compact with a better resistance to environmental changes.

The remainder of this paper is organized as follows. In Section II, the principle of chirped millimeter-wave pulse generation based on spectral shaping and nonlinear frequency-to-time mapping is discussed. An approximate model to describe the frequency characteristics of the generated pulse is also developed. In Section III, a simple and efficient technique to fabricate an NL-CFBG with tunable high-order dispersion is proposed; a theoretical analysis of the dispersion properties in the NL-CFBG is also presented. In Section IV,

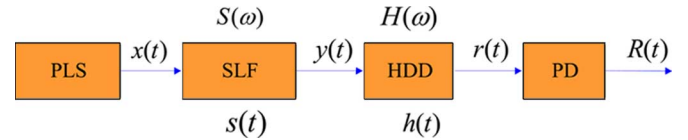


Fig. 1. Schematic diagram of the proposed chirped millimeter-wave pulse generation system. Pulsed laser source: PLS; Sagnac loop filter: SLF; high-order dispersive device: HDD; photodetector: PD.

experimental implementations are carried out to verify the proposed technique. A discussion on the modulation depth of the generated waveform is presented in Section V. A conclusion is drawn in Section VI.

## II. SYSTEM CONFIGURATION AND THEORETICAL ANALYSIS

Optical generation of electrical pulses based on optical spectral shaping and dispersion-induced frequency-to-time mapping has been intensively studied recently with an emphasis on the generation of electrical pulses at high frequencies [5], [6]. The generated microwave or millimeter-wave pulses are usually not chirped. For many applications, it is highly desirable that the pulses are highly chirped in order to implement pulse compression at a receiver. Chirped electrical pulses can be generated based on spectral shaping and frequency-to-time mapping using either a chirped spectral filter with linear frequency-to-time mapping or a uniform spectral filter with nonlinear frequency-to-time mapping. The technique presented here is based on nonlinear frequency-to-time mapping. In the proposed approach, the spectrum of a broadband ultrashort pulse is shaped by an all-fiber two-tap Sagnac loop filter that has a sinusoidal spectral response. The nonlinear frequency-to-time mapping is then implemented using a dispersive device with both tunable first- and second-order dispersion. As a result, a high-frequency chirped electrical pulse can be generated with a tunable central frequency and chirp rate.

The operation principle of the proposed techniques is illustrated in Fig. 1. The system consists of an ultrashort pulsed laser source, a two-tap Sagnac loop filter, a high-order dispersive device, and a high-speed photodetector. In our analysis, both the first- and second-order dispersion are considered.

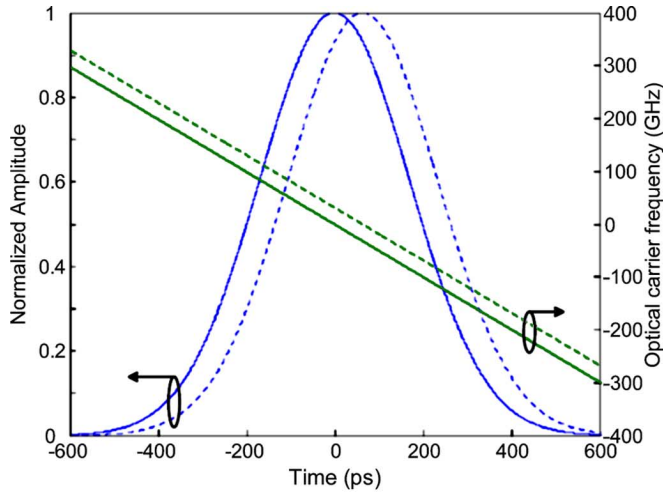
Theoretically, we can assume that the optical pulse from the pulsed laser source is a transform-limited Gaussian pulse with an amplitude  $A_0$ , a carrier angular frequency  $\omega_0$ , and a half pulsewidth  $t_0$  at the  $1/e$  maximum. The envelop of the optical pulse can be expressed as

$$x(t) = A_0 \exp\left(-\frac{t^2}{t_0^2}\right). \quad (1)$$

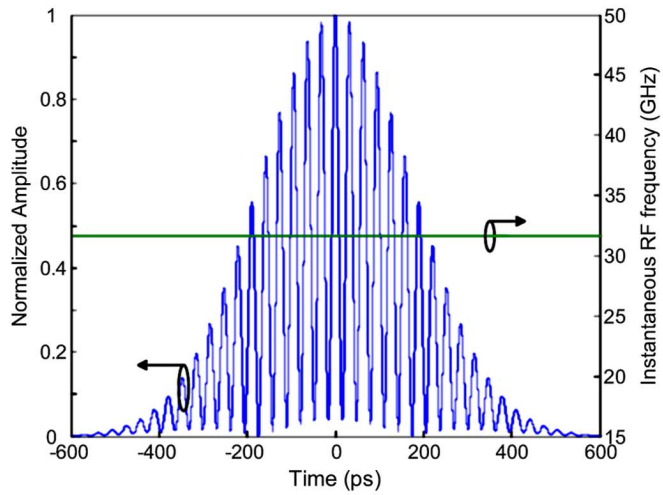
In the system, the Sagnac loop filter with a single length of polarization maintaining fiber can be modeled as a two-tap delay-line filter with an impulse response given by

$$s(t) = \frac{1}{2} [\delta(t) + \delta(t - \tau_0)] \quad (2)$$

where  $\tau_0$  is the time-delay difference. The Sagnac loop filter can be considered as a linear time-invariant (LTI) filter, after propagating through the filter, the envelop of the spectrum-shaped



(a)



(b)

Fig. 2. Simulation results for a chirped millimeter-wave pulse generation system using a dispersive device with the first-order dispersion only. (a) Envelope and optical carrier frequency of the two chirped optical pulses [solid line:  $r_1(t)$ , dotted line:  $r_2(t)$ ]. (b) Amplitude and RF carrier frequency of the generated millimeter-wave pulse.

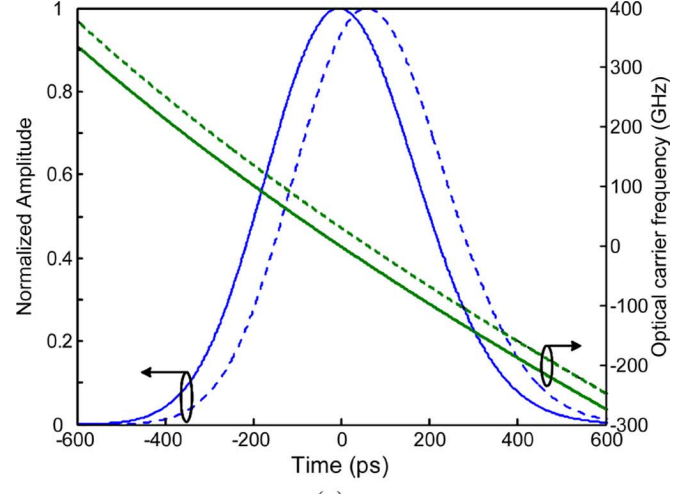
optical pulse,  $y(t)$ , is given by calculating the convolution

$$y(t) = x(t) * s(t) = \frac{1}{2} A_0 \left[ \exp\left(-\frac{t^2}{t_0^2}\right) + \exp\left(-\frac{(t - \tau_0)^2}{t_0^2}\right) \right] \quad (3)$$

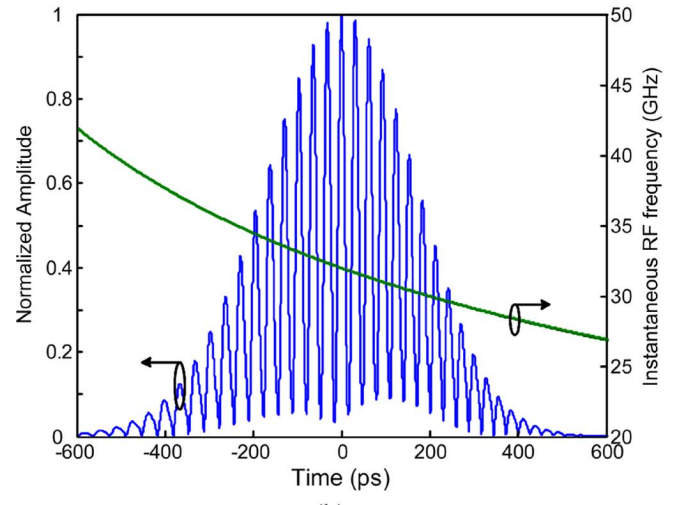
where  $*$  denotes convolution operation.

The spectrum-shaped optical pulse is then sent to a dispersive device, which can also be modeled as an LTI system with a transfer function  $H(\omega) = |H(\omega)| \exp[-j\Phi(\omega)]$ . The phase response of the transfer function, namely,  $\Phi(\omega)$ , can be expanded in the vicinity of the central frequency  $\omega_0$ . Assume that the third-order and higher order dispersion are negligible within the pulse spectral bandwidth, the transfer function  $H(\omega)$  can then be approximated as

$$H(\omega) = |H(\omega)| \exp\left[-j\left(\frac{1}{2}\ddot{\Phi}\omega^2 + \frac{1}{6}\dddot{\Phi}\omega^3\right)\right] \quad (4)$$



(a)



(b)

Fig. 3. Simulation results for a chirped millimeter-wave pulse generation system using a dispersive device with both the first- and second-order dispersion. (a) Envelope and optical carrier frequency of the two chirped optical pulses [solid line:  $r_1(t)$ , dotted line:  $r_2(t)$ ]. (b) Amplitude and RF carrier frequency of the generated millimeter-wave pulse.

where  $\ddot{\Phi} = d^2\Phi(\omega)/d\omega^2|_{\omega=\omega_0}$  and  $\dddot{\Phi} = d^3\Phi(\omega)/d\omega^3|_{\omega=\omega_0}$  are the first- and second-order dispersion coefficients, respectively. Note that  $\omega$  is the relative angular frequency with respect to the central frequency of the optical carrier. Since we mainly focus on the pulse-shape change due to the dispersion effect, the so-called retarded frame is used and the average group delay is ignored [15]. It is important to note that the approximation in (4) is good when the higher order dispersion within the pulse spectral bandwidth satisfies

$$|\ddot{\Phi}\omega^4/24| \ll \pi \quad (5)$$

where  $\ddot{\Phi} = d^4\Phi(\omega)/d\omega^4|_{\omega=\omega_0}$  is the third-order dispersion coefficient.

Let  $r(t)$  be the complex envelope of the output optical pulse from the dispersive device. The Fourier transform of  $r(t)$  is then

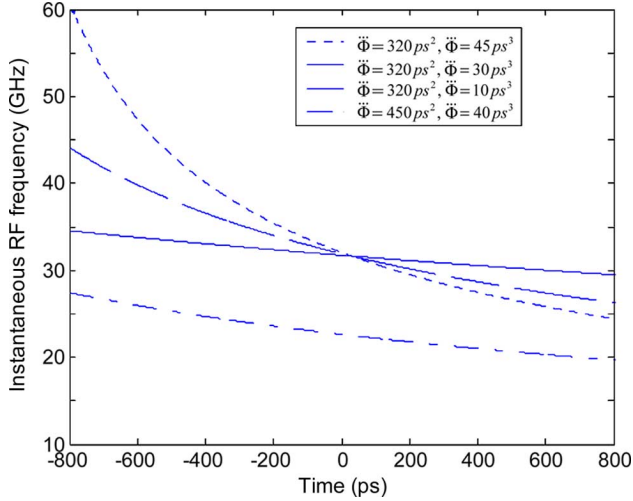


Fig. 4. Instantaneous RF frequency of the generated chirped pulses under different first- and second-order dispersion.

written as

$$\begin{aligned} \tilde{R}(\omega) &= \tilde{Y}(\omega)H(\omega) \\ &= \frac{1}{2}A_0 |H(\omega)| \sqrt{\pi}\tau_0 \exp\left(-\frac{\tau_0^2}{4}\omega^2\right) \\ &\quad \times [1 + \exp(-j\omega\tau_0)] \exp\left[-j\left(\frac{1}{2}\ddot{\Phi}\omega^2 + \frac{1}{6}\ddot{\ddot{\Phi}}\omega^3\right)\right] \end{aligned} \quad (6)$$

where  $\tilde{Y}(\omega)$  is the Fourier transform of  $y(t)$ . The related temporal pulse envelope  $r(t)$  can then be obtained by taking the inverse Fourier transform

$$r(t) = \tilde{F}^{-1}[\tilde{R}(\omega)] = r_1(t) + r_2(t) \quad (7)$$

where

$$\begin{aligned} r_1(t) &= \frac{A_0 |H(\omega)| \tau_0}{4\sqrt{\pi}} \\ &\quad \times \int_{-\infty}^{\infty} \exp\left(-\frac{\tau_0^2}{4}\omega^2 - \frac{j}{2}\ddot{\Phi}\omega^2 - \frac{j}{6}\ddot{\ddot{\Phi}}\omega^3 + j\omega t\right) d\omega \end{aligned} \quad (8a)$$

$$\begin{aligned} r_2(t) &= \frac{A_0 |H(\omega)| \tau_0}{4\sqrt{\pi}} \\ &\quad \times \int_{-\infty}^{\infty} \exp\left[-\frac{\tau_0^2}{4}\omega^2 - \frac{j}{2}\ddot{\Phi}\omega^2 - \frac{j}{6}\ddot{\ddot{\Phi}}\omega^3 + j\omega(t-\tau_0)\right] d\omega. \end{aligned} \quad (8b)$$

An analytic solution of the above integrals can be obtained in terms of the Airy function [15]. It is known that although the incident pulse  $y(t)$  is unchirped, the output optical pulse from the dispersive element  $r(t)$  becomes chirped (with phase modulation).  $r_1(t)$  and  $r_2(t)$  can then be rewritten as

$$r_i(t) = |r_i(t)| \exp[j\phi_i(t)], \quad i = 1, 2 \quad (9)$$

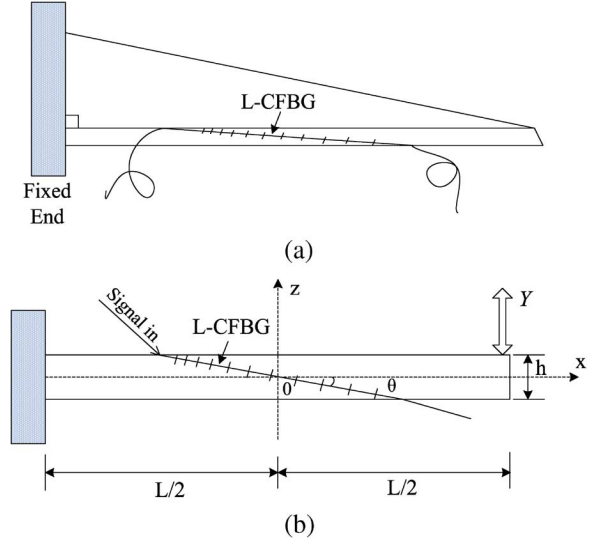


Fig. 5. Schematic diagram showing the NL-CFBG generation using strain-gradient beam tuning technique. (a) Right-angled triangle cantilever beam. (b) Bending of the grating with the beam. Linearly chirped fiber Bragg grating: L-CFBG (from [12]).

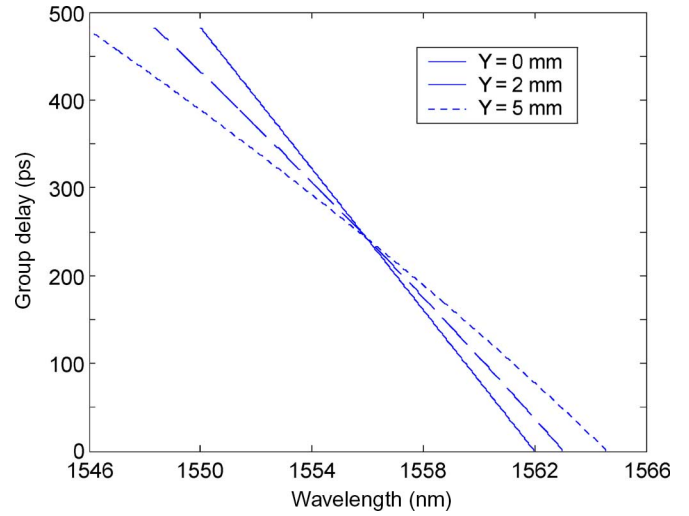


Fig. 6. Simulation results: group-delay characteristics of the generated NL-CFBG at different beam displacements.

where  $\phi_i(t)$  is the time-dependent phase term. Accordingly, the instantaneous carrier frequency of the chirped optical pulses is time dependent as well, which is given by

$$f_i(t) = \frac{1}{2\pi} \frac{d\phi_i(t)}{dt}, \quad i = 1, 2. \quad (10)$$

The two chirped optical pulses  $r_1(t)$  and  $r_2(t)$  are then interfered at a photodetector. The electrical current at the output of the photodetector is proportional to the intensity of the input electrical field, which is expressed as

$$\begin{aligned} R(t) \propto |r(t)|^2 &= |r_1(t)|^2 + |r_2(t)|^2 \\ &\quad + 2|r_1(t)||r_2(t)| \cos[\phi_1(t) - \phi_2(t)]. \end{aligned} \quad (11)$$

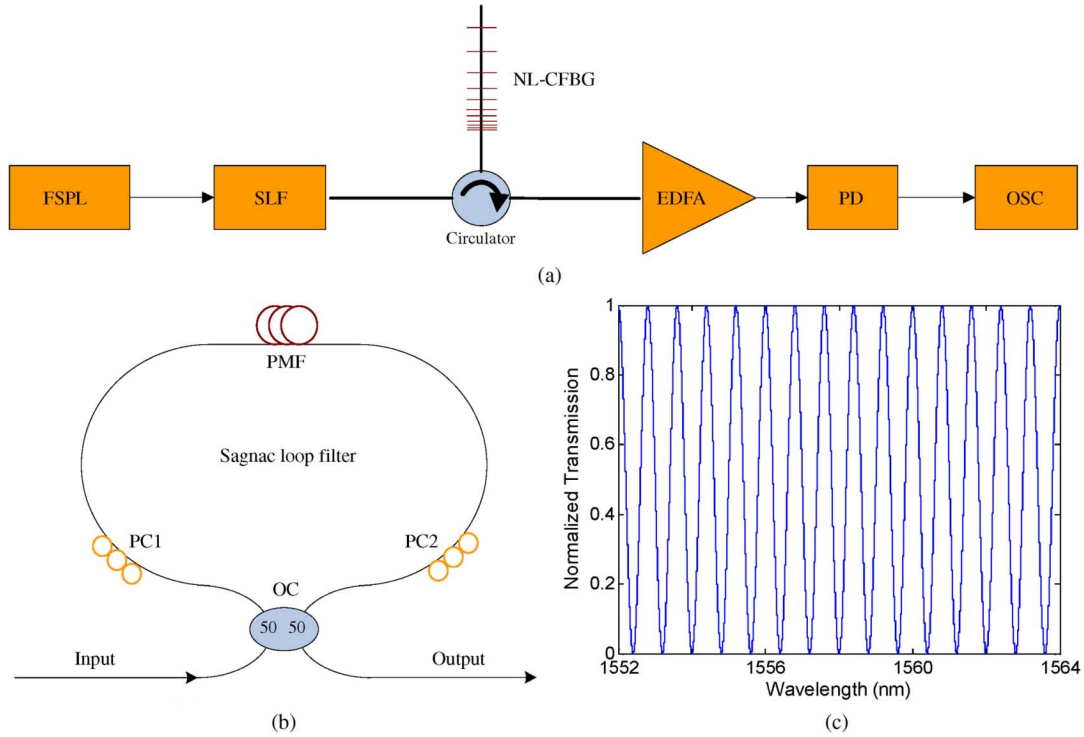


Fig. 7. Experimental setup of the proposed system. (a) System configuration. (b) Two-tap SLF. (c) Normalized transmission response of the SLF. Femtosecond pulsed laser: FSPL; Sagnac loop filter: SLF; nonlinearly chirped fiber Bragg grating: NL-CFBG; erbium-doped fiber amplifier: EDFA; photodetector: PD; optical coupler: OC; polarization controller: PC; polarization maintaining fiber: PMF; oscilloscope: OSC (from [12] and [13]).

It can be seen from (11) that the first and second terms on the right-hand side are the low-frequency components, whereas the third term is the high-frequency component with an instantaneous RF frequency given by

$$f_{\text{RF}}(t) = \frac{1}{2\pi} \frac{d}{dt} [\phi_1(t) - \phi_2(t)] = f_1(t) - f_2(t). \quad (12)$$

Therefore, the beating between the two chirped optical pulses  $r_1(t)$  and  $r_2(t)$  leads to the generation of a chirped millimeter-wave pulse with an instantaneous RF carrier frequency determined by the optical carrier frequency difference of the two optical pulses. According to the above analysis, both the pulse envelope and instantaneous RF carrier frequency of the generated chirped millimeter-wave pulse can be computed by using (8)–(12).

In order to investigate the direct relationship between the dispersion and frequency profile of the generated chirped millimeter-wave pulse, an approximate model focusing on the instantaneous carrier frequency of the generated millimeter-wave pulse is developed based on frequency-to-time mapping.

It is known that the transfer function of a two-tap Sagnac loop filter is given by

$$\tilde{S}(\omega) = \tilde{F}[s(t)] = \frac{1}{2} [1 + \cos(\omega\tau_0)] \quad (13)$$

where  $\tilde{F}(\cdot)$  denotes the Fourier transform operation. The optical intensity spectrum of the spectrum-shaped pulse at the output of the filter can then be expressed as

$$\tilde{Y}(\omega) = |\tilde{X}(\omega)\tilde{S}(\omega)| = \frac{1}{2} \exp\left(-\frac{\tau_0^2}{4}\omega^2\right) [1 + \cos(\omega\tau_0)]. \quad (14)$$

After the spectrum-shaped optical pulse propagates through the dispersive device, where the first- and second-order dispersion are both considered, the spectrum  $\tilde{Y}(\omega)$  is mapped into a temporal waveform  $r(t)$ . Thanks to the high-order dispersion, the frequency-to-time conversion is no longer linear. The non-linear mapping relationship from the frequency domain to time domain is derived from the group delay of the dispersive element and is given by [10]

$$\omega(t) = \frac{-\ddot{\Phi} \pm \sqrt{\ddot{\Phi}^2 + 2\ddot{\Phi}t}}{\ddot{\Phi}} \quad (15)$$

where the  $\pm$  sign is due to the positive or negative dispersion. The mapped temporal waveform is then expressed as

$$\begin{aligned} |r(t)| &\propto |\tilde{Y}(\omega)| \\ &= \frac{-\ddot{\Phi} \pm \sqrt{\ddot{\Phi}^2 + 2\ddot{\Phi}t}}{\ddot{\Phi}} \\ &= \frac{1}{2} \exp\left[-\frac{\tau_0^2}{4} \left(\frac{-\ddot{\Phi} \pm \sqrt{\ddot{\Phi}^2 + 2\ddot{\Phi}t}}{\ddot{\Phi}}\right)^2\right] \\ &\quad \times \left[1 + \cos\left(\frac{\sqrt{\ddot{\Phi}^2 + 2\ddot{\Phi}t}}{\ddot{\Phi}}\tau_0 \pm \frac{\ddot{\Phi}}{\ddot{\Phi}}\tau_0\right)\right]. \end{aligned} \quad (16)$$

From (16), we can find that the instantaneous RF angular frequency of the generated electrical pulse is obtained by

$$\omega_{\text{RF}}(t) = \frac{d}{dt} \left( \frac{\sqrt{\ddot{\Phi}^2 + 2\ddot{\Phi}t}}{\ddot{\Phi}}\tau_0 \pm \frac{\ddot{\Phi}}{\ddot{\Phi}}\tau_0 \right) = \frac{\tau_0}{\sqrt{\ddot{\Phi}^2 + 2\ddot{\Phi}t}}. \quad (17)$$

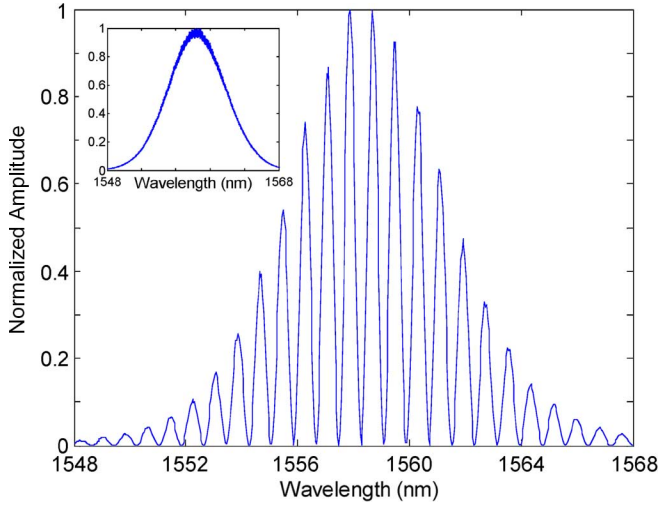


Fig. 8. Optical spectrum of the shaped optical pulse. The inset shows the spectrum of input optical pulse before spectral shaping (data from [12]).

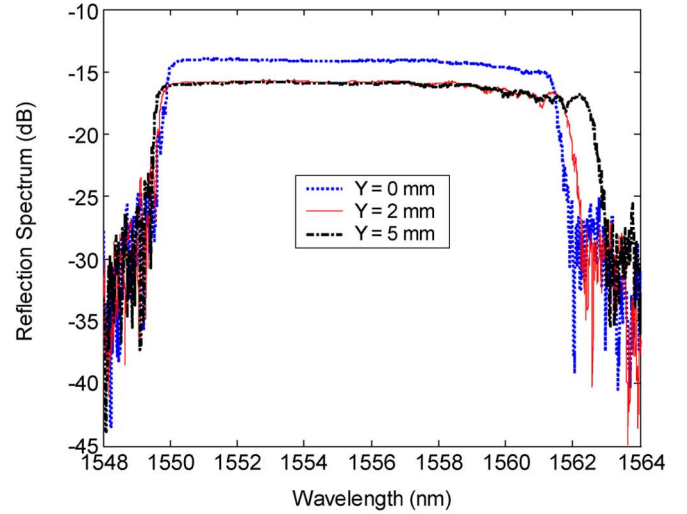
It can be obviously seen from (17) that the generated electrical pulse is nonlinearly chirped. If the dispersion coefficients satisfy that  $|(2\ddot{\Phi})/\ddot{\Phi}^2| \ll 1$ , (17) can be well approximated according to the binomial theorem

$$\omega_{\text{RF}}(t) \cong \frac{\tau_0}{\ddot{\Phi}} - \frac{\ddot{\Phi} \tau_0}{|\ddot{\Phi}|^3} t. \quad (18)$$

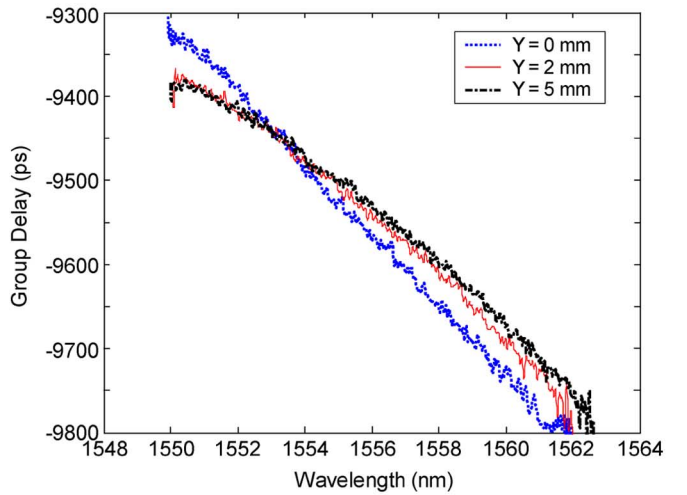
The central frequency of the generated chirped pulse can now be calculated by letting  $t = 0$  in (18), which is  $\omega_0 = \omega_{\text{RF}}(0) = \tau_0/|\ddot{\Phi}|$ . As can be seen, the central frequency is only dependent upon the first-order dispersion coefficient. On the other hand, the instantaneous frequency chirp rate, which is given by  $C_{\text{RF}} = d\omega_{\text{RF}}(t)/dt \cong \ddot{\Phi} \tau_0/\ddot{\Phi}^3$ , is determined by both the first- and high-order dispersion.

To evaluate the approximate model given in (17), numerical simulations are performed based on (8)–(12). In the simulations, the input optical pulsewidth is 550 fs and the FSR of the Sagnac loop filter is chosen to be 0.8 nm, which corresponds to a time-delay difference of  $\tau_0 = 63.6$  ps. In the first example, only the first-order dispersion of  $\ddot{\Phi} = 320$  ps<sup>2</sup> is considered. After propagating through the dispersive device, the two optical pulses are linearly chirped with the same chirp rate, as shown in Fig. 2(a). As a result, the beating of the two delayed and equally chirped optical pulses leads to the generation of an electrical pulse with a constant RF carrier frequency of 31.6 GHz, as shown in Fig. 2(b), which matches well with the prediction given by (17) for  $\ddot{\Phi} = 0$ .

In the second example, both the first- and second-order dispersion are considered. We choose the second-order dispersion  $\ddot{\Phi}$  to be 35 ps<sup>3</sup>, while keeping the first-order dispersion  $\ddot{\Phi}$  to be 320 ps<sup>2</sup>. The simulation results are shown in Fig. 3. Due to the second-order dispersion, the two incident optical pulses are nonlinearly chirped, as shown in Fig. 3(a). Therefore, the beating between the two delayed and nonlinearly chirped optical pulses leads to the generation of a chirped millimeter-wave



(a)



(b)

Fig. 9. Measured: (a) reflection spectrum and (b) group delay of the generated NL-CFBG under different beam deflections (dotted line: zero deflection; solid line: 2-mm deflection; dashed-dotted line: 5-mm deflection).

pulse with the RF carrier frequency given by (12). Simulation results about the generated electrical pulse are shown in Fig. 3(b). In this case, the central frequency is around 31.7 GHz and the instantaneous RF frequency varies from 25.4 to 46.5 GHz within the main pulsewidth, which is in good agreement with the prediction given by (17) as well. The envelope of the generated electrical pulse has a shape close to a Gaussian pulse, but with a slight asymmetry. Simulations show that with a larger second-order dispersion, the pulse envelope becomes more asymmetrical. A detailed analysis on the pulse-shape asymmetry due to higher order dispersion can be found in [16] and [17].

Fig. 4 shows the simulation results of the instantaneous RF frequency of the generated chirped electrical pulses under different first- and second-order dispersion. As can be seen from Fig. 4, by selecting a dispersive device with suitable first- and second-order dispersion, the chirped electrical pulse with the required central frequency and chirp rate can be generated. It is worth noting that a linear frequency chirping is not always necessary in a pulse compression system. In fact, the frequency

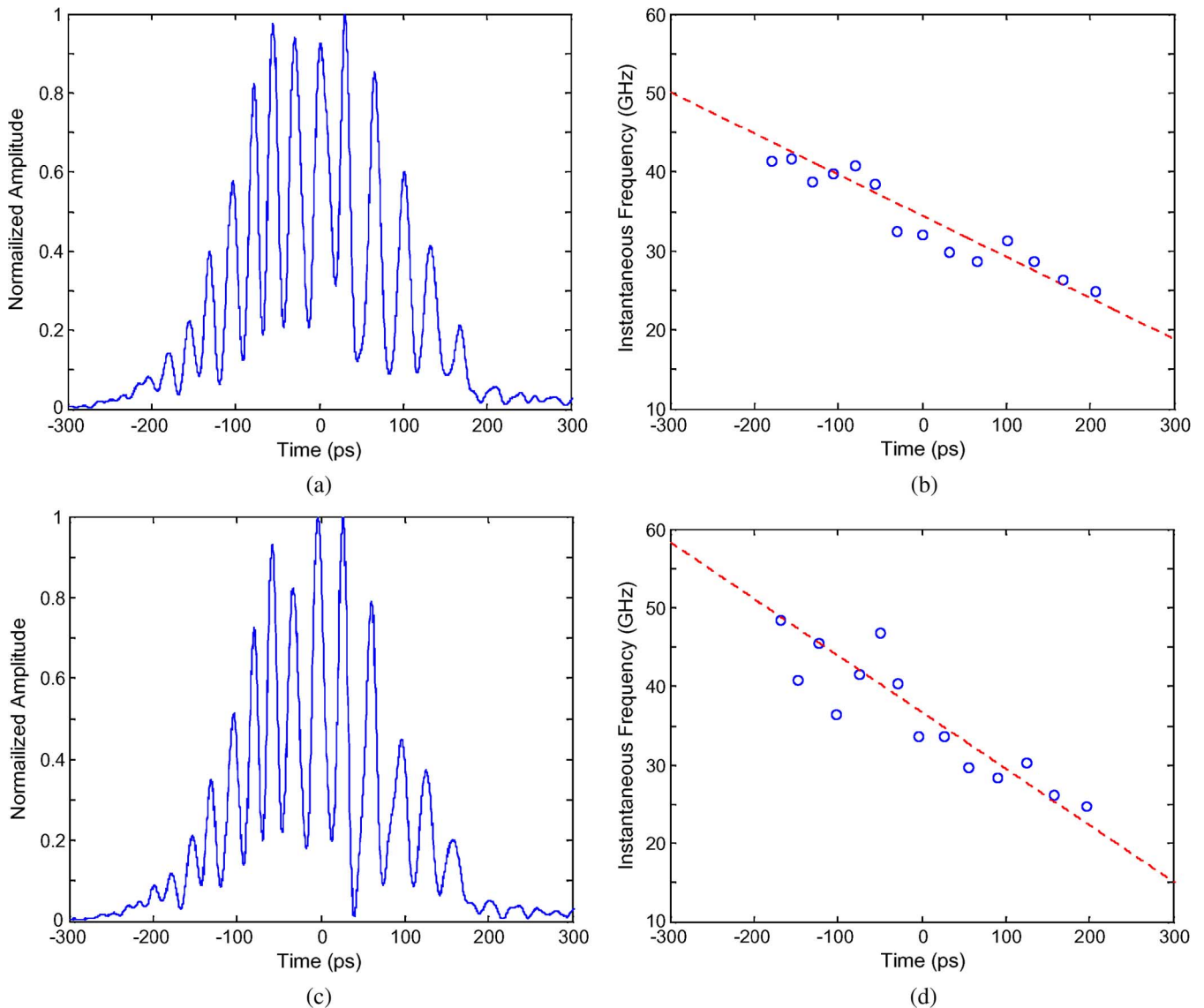


Fig. 10. Experimental results. (a) Pulse profile and (b) instantaneous frequency in the case of 2-mm beam deflection. (c) Pulse profile and (d) instantaneous frequency in the case of 5-mm beam deflection [circle in (b) and (d): obtained from experimental results, dashed line in (b) and (d): theoretical prediction by (18)].

modulation can be of almost any form, provided that the matched filter in the receiver is properly designed to match the transmitted chirped pulse.

### III. NL-CFBG

In the proposed system, a dispersive device with tunable high-order dispersion provides the possibility of tailoring the frequency characteristics of the generated chirped millimeter-wave pulses. Such tunable high-order dispersion is realized by using a properly designed NL-CFBG, in which the group-delay response varies nonlinearly with respect to the optical wavelength. NL-CFBGs have been widely used to compensate for high-order chromatic dispersion and polarization mode dispersion in high-speed optical communications systems [18]–[20]. NL-CFBGs were usually fabricated using a nonlinearly chirped phase mask [19] or a linearly chirped phase mask with a properly controlled exposure time during the fabrication to introduce a nonlinear

chirp [18]. These fabrication techniques are either expensive or complicated. It is, therefore, highly desirable to develop a simple and low-cost technique for the NL-CFBG fabrication.

In this paper, we propose a simple and efficient method to introduce large nonlinear chirp to a regular linearly chirped fiber Bragg grating based on strain-gradient beam tuning. Fig. 5 shows the schematic diagram of the NL-CFBG fabrication technique. As can be seen from Fig. 5(a), a linearly chirped fiber Bragg grating is glued in an inclined direction onto the lateral side of a right-angled triangular cantilever beam. When a mechanical force is applied to the free end of the beam, as shown in Fig. 5(b), a linear strain gradient is generated, which leads to the generation of an NL-CFBG.

In Fig. 5(b), the  $x$ -axis is on the neutral layer of the beam,  $L$  is the beam length,  $h$  is the thickness of the beam,  $\theta$  is the angle between the grating axis and the beam neutral surface, and  $Y$  is the applied displacement at the free end of the beam. The center of the grating is consistent with the neutral layer on the side

cross section. This ideal situation will be always considered in the following analysis.

When the beam is bent by deflecting the free end while keeping the other end fixed, the introduced axial strain gradient along the grating can be expressed as [11]

$$\varepsilon_{\text{axis}}(l) = \frac{1}{2}\kappa l \sin(2\theta) = \frac{Y \sin(2\theta)}{L^2}l \quad (19)$$

where  $\kappa$  is the beam curvature, and  $l$  is the grating length between the given point and the center point of grating. Assume that  $\theta$  is approximately constant, which is true if the beam displacement is small relative to the length of beam. It can be seen from (19) that the linear strain is produced along the grating when deflecting the beam. Suppose that the deflection is upward ( $Y > 0$ ), then the strain on the neutral layer of the beam is zero; half of the grating (the section of  $0 < x < L/2$ ) is under varying tension strain, whereas the other half (the section of  $-L/2 < x < 0$ ) suffers a varying compression strain. The symmetrical strain distribution ensures that the central wavelength of the grating may keep closely fixed during the beam tuning process.

When a linearly chirped fiber Bragg grating is mounted on the side surface of the beam, the developed linear strain gradient is transferred to physically change the grating pitch according to the strain-optic effect. The grating pitch variance  $\Delta\Lambda$  is expressed as

$$\Delta\Lambda(l) = (1-p_e)\varepsilon_{\text{axis}}(l)\Lambda(l) = (1-p_e)\frac{Y \sin(2\theta)}{L^2}(\Lambda_C + R_\Lambda l)l \quad (20)$$

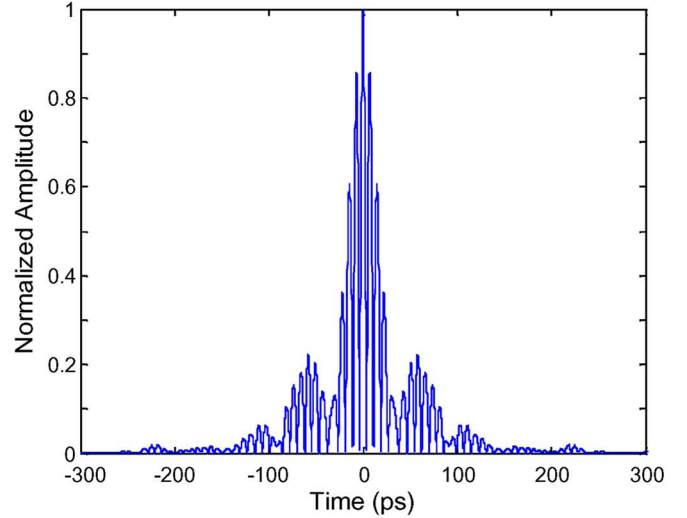
where  $p_e$  is the effective photo-elastic constant ( $\sim 0.22$ ) of the fiber material,  $\Lambda_C$  is the central grating pitch, and  $R_\Lambda$  is the chirp rate of the grating pitch.

According to the well-known Bragg condition, the Bragg wavelength distribution  $\lambda_B(l)$  as a function of distance  $l$  along the fiber axis under linear strain gradient is expressed as [12]

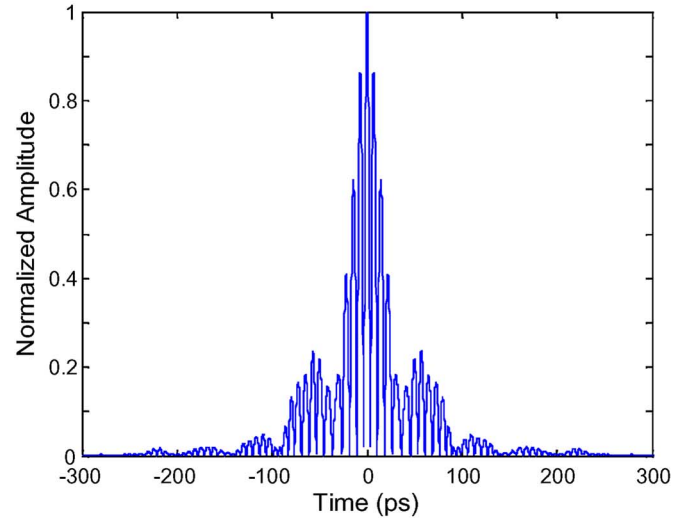
$$\begin{aligned} \lambda_B(l) &= \lambda_{B_C} + K_1 l + K_2 l^2 \\ K_1 &= R_\lambda + \lambda_{B_C} \frac{Y \sin(2\theta)}{L^2} (1-p_e) \\ K_2 &= R_\lambda \frac{Y \sin(2\theta)}{L^2} (1-p_e) \end{aligned} \quad (21)$$

where  $\lambda_{B_C}$  is the center wavelength of the linearly chirped fiber Bragg grating and  $R_\lambda$  (nm/mm) is the wavelength chirp rate of the original grating. It is shown that the Bragg wavelength distribution is a quadratic function of the distance  $l$ , instead of a linear function, as in a linearly chirped fiber Bragg grating. Consequently, an NL-CFBG with a nonlinear group delay is fabricated directly from a regular linearly chirped fiber Bragg grating by applying linear strain gradient.

Fig. 6 shows the calculated group delays of the NL-CFBG with different displacements according to the method presented in this paper. In our simulation, the length of the cantilever beam is chosen to be 150 mm, and the grating angle is  $\theta = 15^\circ$ . An initial linearly chirped fiber Bragg grating with a grating length of 50 mm, a center Bragg wavelength of  $\lambda_{B_C} = 1556$  nm, and a linear chirp rate of  $R_\lambda = 0.24$  nm/mm is considered. Without loss of generality, we assume that the grating reflects a longer



(a)



(b)

Fig. 11. Autocorrelation waveforms of the generated chirped millimeter-wave pulses. (a) Beam displacement is 2 mm. (b) Beam displacement is 5 mm.

wavelength at the input end and a shorter wavelength at the back end, therefore, the grating has a negative first-order dispersion. In fact, for an initially unchirped optical incident pulse, dispersion-induced broadening and phase modulation of the pulse does not depend on the sign of the first-order dispersion coefficient  $\ddot{\Phi}$  [15]. It is obviously shown in Fig. 6 that the nonlinear chirp characteristics of the NL-CFBG can be easily controlled by adjusting one parameter only, namely, the beam deflection  $Y$ . For example, for the case of displacement  $Y = 2$  mm, the equivalent first- and second-order dispersion coefficients of the generated NL-CFBG at 1556 nm are  $\ddot{\Phi} = 265.4$  ps<sup>2</sup> and  $\ddot{\ddot{\Phi}} = 24.7$  ps<sup>3</sup>, respectively. If the displacement  $Y$  is increased to 5 mm, the first- and second-order dispersion coefficients will become  $\ddot{\Phi} = 209.4$  ps<sup>2</sup> and  $\ddot{\ddot{\Phi}} = 29.6$  ps<sup>3</sup> at 1556 nm.

There is a tradeoff between the nonlinearity and dispersion: a larger group delay nonlinearity and a broader spectral bandwidth can be realized when a larger displacement is applied, but a decreased dispersion level would be resulted. By properly

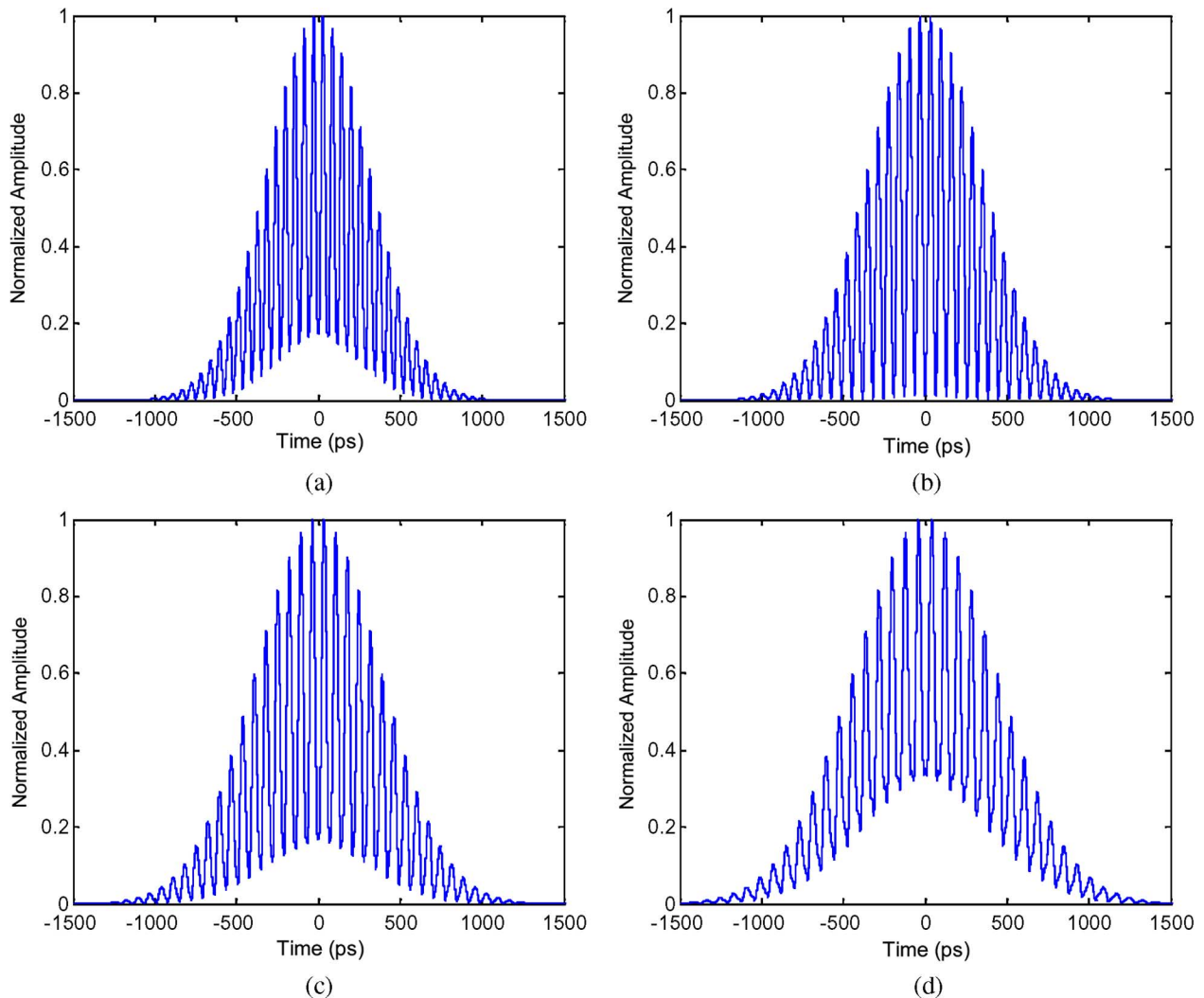


Fig. 12. Generated waveforms with different modulation depth under different first-order dispersion. (a) 580, (b) 648, (c) 700, and (d) 820 ps<sup>2</sup>.

choosing the displacement  $Y$ , the NL-CFBG can provide a sufficiently large dispersion, a suitable nonlinear group delay and bandwidth for the application in generating chirped electrical pulses, as described in this paper.

#### IV. EXPERIMENT

An experiment is carried out to verify the proposed approach for chirped millimeter-wave pulses generation. The experimental setup of the proposed system is shown in Fig. 7(a). A femtosecond pulsed laser is used to generate a broadband transform-limited ultrashort Gaussian pulse. A two-tap Sagnac loop filter, which consists of a length of polarization maintaining fiber and two polarization controllers, as shown in Fig. 7(b), serves as an optical spectral filter. The Sagnac loop filter has a uniform sinusoidal spectral response, as shown in Fig. 7(c). The FSR is determined by the length and the birefringence of the polarization maintaining fiber. An NL-CFBG is used as a dispersive device with both the first- and second-order dispersion, which is fabricated based on our proposed beam-bending technique, to perform the nonlinear frequency-to-time mapping. As a result, a chirped millimeter-wave pulse is obtained at the output of a high-speed photodetector.

In the experiment, a transform-limited Gaussian pulse with a full width at half maximum (FWHM) of 550 fs is used as the input pulse. The central wavelength of the ultrashort pulse is 1558.5 nm, and the 3-dB spectral bandwidth is 8 nm, as shown in the inset of Fig. 8. The FSR of the Sagnac loop filter is set as 0.8 nm. After the spectral shaping by the filter, we obtain a spectrum-shaped pulse with its spectrum shown in Fig. 8.

The performance of the fabricated NL-CFBG is measured first. In order to cover the main spectrum bandwidth of the broadband femtosecond laser source, a regular linearly chirped fiber Bragg grating with a linear chirp rate of 0.24 nm/mm, grating length of 50 mm, and center Bragg wavelength of 1556 nm is used to generate an NL-CFBG based on the strain-gradient beam tuning technique, as described in Section III.

Fig. 9 shows the measured reflection spectra and group delays of the produced NL-CFBG under different beam free end deflections. It is seen from Fig. 9(a) that the 3-dB spectral bandwidth can be tuned from 11.6 nm (with zero displacement) to 13.2 nm. In order to cover the spectrum of the optical pulse as much as possible, the grating center point is intentionally mismatched with the beam neutral layer: a major part of the grating

experiences the tension strain and a minor part of the grating experiences the compression strain. As a result, the central wavelength of the produced NL-CFBG is slightly shifted to a longer wavelength when bending the beam. In the meantime, a nonlinear group-delay distribution with respect to the wavelength is realized as well, as shown in Fig. 9(b). We can find that a larger nonlinearity of the group delay and a broader spectral bandwidth can be achieved in the NL-CFBG when a larger displacement is applied, which is consistent with the theoretical analysis in Section III.

The experimental results are shown in Fig. 10. Both the pulse profile and instantaneous frequency versus time are shown. In the first example, the applied beam deflection is 2 mm. According to the measured group-delay result, the equivalent first- and second-order dispersion coefficients  $\ddot{\Phi}$  and  $\ddot{\Phi}^*$  at 1558.5 nm are 295.1 ps<sup>2</sup> and 20.9 ps<sup>3</sup>, respectively. Thanks to the nonlinear frequency-to-time mapping, a chirped millimeter-wave pulse is generated. As can be seen from Fig. 10(a), the FWHM of the generated pulse envelope is around 243 ps, which is measured by a high-speed sampling oscilloscope (Agilent 86100C). Fig. 10(b) shows the instantaneous RF frequency within the main pulsewidth, which can be calculated by Hilbert transform [21]. Here, for simplicity, the instantaneous frequency is approximated by the reciprocal of the time period of pulse trace, as shown by the solid circle curve. The dotted curve illustrates the theoretical prediction given by (18). In this case, the frequency profile of the generated millimeter-wave pulse is quasi-linear and the instantaneous frequency changes from 25 to 43 GHz, which corresponds to an equivalent frequency chirp rate of 0.053 GHz/ps. In the second case, the beam displacement is increased to 5 mm, which leads to the equivalent first- and second-order dispersion coefficients of  $\ddot{\Phi} = 278.1$  ps<sup>2</sup> and  $\ddot{\Phi}^* = 23.7$  ps<sup>3</sup> at 1558.5 nm. As a result, the FWHM of the generated pulse envelope is around 218 ps; the instantaneous frequency varies from 24 to 49 GHz, which corresponds to a chirp rate of 0.074 GHz/ps, as shown in Fig. 10(c) and (d). One may notice that the measured instantaneous frequency does not match the theoretical prediction at some time points. This discrepancy is resulted from the abnormal strain induced dispersion variation in the NL-CFBG when applying the beam deflection. One solution to reduce the error is to use a beam with a more smooth surface and more stable strain distribution.

From the above experimental results, we can find that, with larger beam deflection, the fabricated NL-CFBG will possess smaller first-order dispersion, but higher second-order dispersion. As a result, the generated waveform will have a higher central frequency and a larger chirp rate. The system shows its high efficiency of controlling the frequency profile of the generated electrical waveform.

Fig. 11 shows the autocorrelations of the generated millimeter-wave pulses with different chirp rates. In the above two cases (2- and 5-mm beam deflections), the FWHMs of the obtained autocorrelation envelopes are around 49 and 42 ps, respectively. By comparison with the results in Fig. 10, pulse compression ratios of 4.9 and 5.2 are achieved. Despite that the realized pulse compression ratio is not very high due to

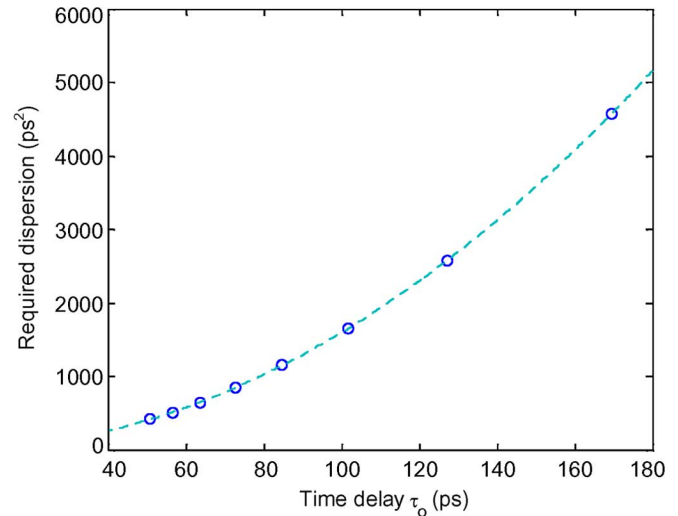


Fig. 13. Required first-order dispersion to generate a temporal waveform with an optimal modulation depth at different time delays (circle: simulation results, dotted line: quadratic fitting result).

the small amount of cycles within the pulse envelope and the limited high-order dispersion in our NL-CFBG, the nonlinear dispersion induced pulse chirping is observed and verified. The experimental results also agree well with the theoretical predictions. In order to achieve a higher pulse compression ratio for practical applications, an optical spectral filter with narrower FSR should be used to generate more cycles within the pulse envelope, and a longer grating should be fabricated to satisfy the requirement of large high-order dispersion and wide bandwidth.

## V. DISCUSSION

According to the principle of dispersion-induced frequency-to-time mapping, the generated temporal waveform should have the same shape with the shaped optical spectrum, as shown in Fig. 8. From the experimental results shown in Fig. 10(a) and (c), however, it is found that the measured time-domain waveforms have a limited modulation depth compared with the shaped optical spectrum. Similar effects have also been found in [6] and [9]. Their analysis indicated that the reduced modulation depth could be caused due to the nonflat frequency response of the photodetector or the environmental changes during the measurement, which could slightly change the interference pattern and cause a decrease of the modulation depth.

In order to find a more intrinsic mechanism that leads to the degradation in the modulation depth of the generated waveforms, some simulations based on the theoretical model presented in Section II are performed. Fig. 12 shows the simulation results, where the FSR of the Sagnac loop filter is chosen as 0.8 nm, or an equivalent time-delay difference of  $\tau_0 = 63.6$  ps. Several cases with different first-order dispersion are considered. For simplicity, the second-order dispersion is not considered since it has negligible contributions to the poor modulation depth, but only slightly distorts the generated waveform.

From Fig. 12 we can find that for two incident optical pulses with a given time-delay difference  $\tau_0$ , only a certain value of dis-

persion can convert the shaped optical spectrum to a temporal waveform with a good modulation depth, as shown in Fig. 12(b). A larger or smaller value of dispersion will lead to a poor modulation depth in the central part of the generated waveform, as shown in Fig. 12(a) and (c). The modulation depth degradation will become more serious if much larger dispersion is applied, as shown in Fig. 12(d). This may be explained by considering the interference effect of two optical pulses. It is known that a stable interference pattern with good interference visibility can be obtained only if the phase difference reaches  $\pi$  and the amplitudes of the two pulses are identical at certain time points. In the dispersion-induced frequency-to-time mapping system, the phase difference and the relative amplitude difference between two optical pulses depend not only on the time-delay difference  $\tau_0$ , but also on the total dispersion experienced by the optical pulses. As a result, for a given  $\tau_0$ , the above ideal interference conditions can be satisfied only at a certain value of dispersion.

Further simulations are performed to find the relationship between the time-delay difference  $\tau_0$  and the required dispersion for realizing an optimal modulation depth. Fig. 13 shows the simulation results. A quadratic relationship between the dispersion  $\ddot{\Phi}$  and the time-delay difference  $\tau_0$  is found as follows:

$$\ddot{\Phi}(\tau_0) = 0.159\tau_0^2 + 0.026\tau_0 + 1.91 \quad (22)$$

which gives us a good prediction for the selection of the required dispersion in designing a chirped electrical pulse generation system.

## VI. CONCLUSION

A detailed theoretical and experimental study on the generation of chirped millimeter-wave pulse with tunable chirp rate based on optical spectral shaping and nonlinear frequency-to-time mapping was performed in the paper. In the system, the spectral shaping was implemented using a two-tap Sagnac loop filter with a uniform sinusoidal spectral response. The nonlinear frequency-to-time mapping was realized by applying the spectrum-shaped pulse to an NL-CFBG with both first- and second-order dispersion. The NL-CFBG was fabricated from a regular linearly chirped fiber Bragg grating using a simple beam-bending technique. By properly controlling the first- and second-order dispersion in the NL-CFBG, the chirped millimeter-wave pulse with required central frequency and chirp rate could be generated.

A detailed theoretical analysis to describe the generation of chirped millimeter-wave pulses was developed. The direct relationship between the dispersion and the frequency profile of the generated chirped pulse was revealed by an approximate model. An experiment was performed to verify the proposed approach. Chirped millimeter-wave pulses with a central frequency of around 35 GHz and instantaneous frequency chirp rates of 0.053 and 0.074 GHz/ps were generated.

A major advantage of the proposed approach is that the frequency characteristics of the generated chirped millimeter-wave pulse could be easily tailored by adjusting the parameters of the system. The demonstrated approach offers a solution to the generation of high-frequency electrical pulse with large tunable

chirp rate for applications in high-speed communications and modern radar systems.

## REFERENCES

- [1] A. W. Rihaczek, *Principles of High-Resolution Radar*. Norwood, MA: Artech House, 1996.
- [2] M. Bertero, M. Miyakawa, P. Boccacci, F. Conte, K. Orikasa, and M. Furutani, "Image restoration in chirp pulse microwave CT (CP-MCT)," *IEEE Trans. Biomed. Eng.*, vol. 47, no. 5, pp. 690–699, May 2000.
- [3] H. D. Griffiths and W. J. Bradford, "Digital generation of high time-bandwidth product linear FM waveforms for radar altimeters," *Proc. Inst. Elect. Eng.*, vol. 139, no. 2, pt. F, pp. 160–169, Apr. 1992.
- [4] H. Kwon and B. Kang, "Linear frequency modulation of voltage-controlled oscillator using delay-line feedback," *IEEE Microw. Wireless Compon. Lett.*, vol. 15, no. 6, pp. 431–433, Jun. 2005.
- [5] J. Chou, Y. Han, and B. Jalali, "Adaptive RF-photonic arbitrary waveform generator," *IEEE Photon. Technol. Lett.*, vol. 15, no. 4, pp. 581–583, Apr. 2003.
- [6] H. Chi, F. Zeng, and J. P. Yao, "Photonic generation of microwave signals based on pulse shaping," *IEEE Photon. Technol. Lett.*, vol. 19, no. 5, pp. 668–670, May 2007.
- [7] C. Wang, F. Zeng, and J. P. Yao, "All-fiber ultrawideband pulse generation based on spectral shaping and dispersion-induced frequency-to-time conversion," *IEEE Photon. Technol. Lett.*, vol. 19, no. 2, pp. 137–139, Feb. 2007.
- [8] M. A. Muriel, J. Azaña, and A. Carballar, "Real-time Fourier transformer based on fiber gratings," *Opt. Lett.*, vol. 24, no. 1, pp. 1–3, Jan. 1999.
- [9] A. Zeitouny, S. Stepanov, O. Levinson, and M. Horowitz, "Optical generation of linearly chirped microwave pulses using fiber Bragg gratings," *IEEE Photon. Technol. Lett.*, vol. 17, no. 3, pp. 660–662, Mar. 2005.
- [10] H. Chi and J. P. Yao, "All-fiber chirped microwave pulse generation based on spectral shaping and wavelength-to-time conversion," *IEEE Trans. Microw. Theory Tech.*, vol. 55, no. 9, pp. 1958–1963, Sep. 2007.
- [11] X. Dong, P. Shum, N. Q. Ngo, C. C. Chan, J. H. Ng, and C.-L. Zhao, "Largely tunable CFBG-based dispersion compensator with fixed center wavelength," *Opt. Express*, vol. 11, no. 22, pp. 2970–2974, Nov. 2003.
- [12] C. Wang and J. P. Yao, "All-optical electrical chirped pulse generation based on nonlinear wavelength-to-time conversion in a chirped fiber Bragg grating," *Proc. SPIE*, vol. 6796, 2007, 67962K.
- [13] C. Wang and J. P. Yao, "All-optical high-frequency electrical chirped pulse generation using a nonlinearly chirped fiber Bragg Grating," in *Int. Signals, Syst., Electron. Symp.*, Montreal, QC, Canada, Jul. 30–Aug. 2 2007, pp. 625–628.
- [14] H. Chi and J. P. Yao, "Chirped RF pulse generation based on optical frequency-to-time mapping using a nonlinearly chirped fiber Bragg grating," *J. Lightw. Technol.*, to be published.
- [15] G. P. Agrawal, *Nonlinear Fiber Optics*, 2nd ed. New York: Academic, 1995.
- [16] M. Miyagi and S. Nishida, "Pulse spreading in a single-mode fiber due to third-order dispersion," *Appl. Opt.*, vol. 18, no. 5, pp. 678–682, Mar. 1979.
- [17] M. Amemiya, "Pulse broadening due to higher order dispersion and its transmission limit," *J. Lightw. Technol.*, vol. 20, no. 4, pp. 591–597, Apr. 2002.
- [18] K. M. Feng, J. X. Cai, V. Grubsky, D. S. Starodubov, M. I. Hayee, S. Lee, X. Jiang, A. E. Willner, and J. Feinberg, "Dynamic dispersion compensation in a 10-Gb/s optical system using novel voltage tuned nonlinearly chirped fiber Bragg grating," *IEEE Photon. Technol. Lett.*, vol. 11, no. 3, pp. 373–375, Mar. 1999.
- [19] S. Lee, R. Khosravani, J. Peng, V. Grubsky, D. S. Starodubov, A. E. Willner, and J. Feinberg, "Adjustable compensation of polarization mode dispersion using a high-birefringence, nonlinearly chirped fiber Bragg grating," *IEEE Photon. Technol. Lett.*, vol. 11, no. 10, pp. 1277–1279, Oct. 1999.
- [20] Z. Pan, Y. W. Song, C. Yu, Y. Wang, Q. Yu, J. Popelek, H. Li, Y. Li, and A. E. Willner, "Tunable chromatic dispersion compensation in 40 Gbit/s systems using nonlinearly chirped fiber Bragg grating," *J. Lightw. Technol.*, vol. 20, no. 12, pp. 2239–2246, Dec. 2002.
- [21] S. Mallet, *A Wavelet Tour of Signal Processing*. San Diego, CA: Academic, 1999.



photonics systems.

**Chao Wang** received the B.Eng. degree in opto-electrical engineering from Tianjin University, Tianjin, China, in 2002, the M.Sc. degree in physics from Nankai University, Tianjin, China, in 2005, and is currently working toward the Ph.D. degree in electrical engineering at the School of Information Technology and Engineering, University of Ottawa, Ottawa, ON, Canada.

His current research interests include microwave signal generation, radio-over-fiber systems, and fiber Bragg gratings and their applications in microwave

Engineering, Nanyang Technological University, Singapore. He holds a guest professorship with Shantou University, Shantou, Guangdong, China, and Sichuan University, Chengdu, Sichuan, China. In 2005, he spent three months as an Invited Professor with the Institut National Polytechnique de Grenoble, Grenoble, France. He has authored or coauthored over 170 papers in refereed journal and conference proceedings. His research has focused on microwave photonics, which includes all-optical microwave signal processing, photonic generation of microwave, millimeter wave, and terahertz, radio-over-fiber, ultra-wideband (UWB) over fiber, fiber Bragg gratings for microwave photonics applications, and optically controlled phased-array antenna. His research interests also include fiber lasers, fiber-optic sensors, and bio-photonics.

Dr. Yao is a Registered Professional Engineer in Ontario, Canada. He is a member of The International Society for Optical Engineers (SPIE) and the Optical Society of America (OSA). He is a senior member of the IEEE Lasers and Electro-Optics Society (LEOS) and the IEEE Microwave Theory and Techniques Society (IEEE MTT-S).



**Jianping Yao** (M'99–SM'01) received the Ph.D. degree in electrical engineering from the Université de Toulon, Toulon, France, in 1997.

In 2001, he joined the School of Information Technology and Engineering, University of Ottawa, Ottawa, ON, Canada, where he is currently a Professor, Director of the Microwave Photonics Research Laboratory, and Director of the Ottawa–Carleton Institute for Electrical and Computer Engineering. From 1999 to 2001, he held a faculty position with the School of Electrical and Electronic